CHINESE OPTICS LETTERS

Vol. 20, No. 9 | September 2022

Spectrally sliced heterodyne coherent receiver with halved electrical bandwidth

Qi Wu (吴 琪), Yixiao Zhu (朱逸萧)*, Ziyu Cheng (程子钰), Longjie Yin (尹龙杰), and Weisheng Hu (胡卫生)**

State Key Laboratory of Advanced Optical Communication Systems and Networks, Department of Electronic Engineering, Shanghai Jiao Tong University, Shanghai 200240, China

*Corresponding author: yixiaozhu@sjtu.edu.cn

**Corresponding author: wshu@sjtu.edu.cn

Received February 15, 2022 | Accepted May 13, 2022 | Posted Online June 15, 2022

A spectrally sliced heterodyne coherent receiver (SHCR) employing four balanced photodetectors and analog-to-digital converters with half of the signal bandwidth is proposed to complete the signal reception and field recovery. We first numerically characterize the performance of SHCR compared with an intradyne coherent receiver and then validate the principle of the SHCR in a proof-of-concept single-polarization experiment. A 60 GBaud 16-quadrature amplitude modulation transmission is experimentally demonstrated over 80 km standard single-mode fiber with a bit-error-rate of 8.5×10^{-4} below the 7% hard-decision forward error correction threshold of 3.8×10^{-3}. The SHCR offers a low-cost, hybrid-free, and channel-skew-tolerant candidate for data center interconnects.

Keywords: sliced heterodyne coherent receiver; heterodyning; spectral slicing; electrical bandwidth.

DOI: 10.3788/COL202220.090601

1. Introduction

Since 2005, digital coherent receivers have brought optical communication into a new era[1]. Optical coherent detection enables full-field recovery of dual-polarization in-phase and quadrature (IQ) modulated signal, quadrupling the transmission spectral efficiency compared with intensity-modulation direct detection (IMDD) solutions. Optical field impairments such as chromatic dispersion (CD) and polarization mode dispersion (PMD) can be also compensated by digital signal processing (DSP) at the receiver[2]. According to the frequency offset between the local oscillator (LO) and the signal, coherent receivers are divided into two categories: heterodyne coherent receiver (HCR) and intradyne coherent receiver (ICR). Intradyne detection has been investigated extensively in optical communication systems[3–5] because it relaxes the requirement for the bandwidth of analog-to-digital converters (ADCs).

To simplify the structure of a standard ICR, one attempt is to replace balanced photodetectors (BPDs) with single-ended photodetectors (SPDs)[6,7], which also proposes low-complexity DSP algorithms to eliminate signal-signal beat interference (SSBI) accordingly. Meanwhile, 3×3 couplers can be employed to achieve a similar function of 90° optical hybrids, which is experimentally demonstrated for $55\lambda \times 112$ Gb/s dual-polarization quadrature-phase-shift-keying signal reception[8].

In comparison, the HCR can reduce the hardware complexity to two BPDs and two ADCs[9], eliminating the use of optical hybrids. Another advantage of the HCR is that one LO laser can be used for two neighboring wavelength division multiplexing (WDM) channels. Therefore, the number of LO lasers can be reduced by half compared to intradyne detection[10]. The electrical bandwidth of photonic integrated circuits (PICs) is the predominant cost of an integrated circuit[11]. However, the critical issue of the HCR, the doubled electrical bandwidth requirement of ADCs and photodetectors (PDs), has not been well resolved.

In the scenario of data center interconnection (DCI), 4/8-lane coarse-WDM (CWDM)-based IMDD systems have been widely adopted[12]. Compared with the IMDD system, coherent detection shows superior dispersion tolerance but relatively higher hardware cost at present. Narrower channel spacing is also allowed in coherent detection systems thanks to the frequency-selective beating with LO. Current coherent optical communication systems all employ arrays of discrete wavelength laser sources as LO. The optical frequency comb (OFC) source has been proposed to replace hundreds of individual lasers with shared cost, aimed at reducing the power consumption and size of the transceivers. In addition, an OFC provides frequency and phase locked comb lines, enabling the advantages over the individual lasers such as reducing guard bands and joint DSP among WDM channels[13].

In this work, we propose a spectrally sliced HCR (SHCR) to relax electrical requirements for ADCs and PDs of a heterodyne

coherent detection system for intra-DCI interconnects and the scenarios with the OFC as a laser source. The proposed SHCR utilizes the two comb lines to halve the required electrical bandwidth in the HCR. Thanks to spectrally sliced detection, the required electrical bandwidth for SHCR is reduced by almost half compared with the conventional HCR. Assisted with OFC and advanced digital processing techniques, the proposed SHCR fully utilizes the electrical bandwidth of the receiver, slightly reducing the hardware cost of coherent detection since it eliminates the utilization of optical hybrids, and the cost induced by OFC is shared equally in all WDM channels.

2. Principle of SHCR and Simulations

The ICR and proposed SHCR are depicted in Figs. 1(a) and 1(b). Figure 1(a) shows the configuration of a standard ICR. As we can see, it requires four BPDs and two optical hybrids to obtain the I/Q information of signals. The comb line demultiplexed from an OFC serves as an LO. The IQ components of the received optical signal with polarization diversity are linearly mapped to the electrical domain by mixing the received optical field with an LO. This direct mapping enables impairments compensation in the receiver DSP, which then allows the use of high-order quadrature amplitude modulation (QAM) formats.

The baseband signal is directly obtained for intradyne detection, so its predominant advantage is the halved electrical

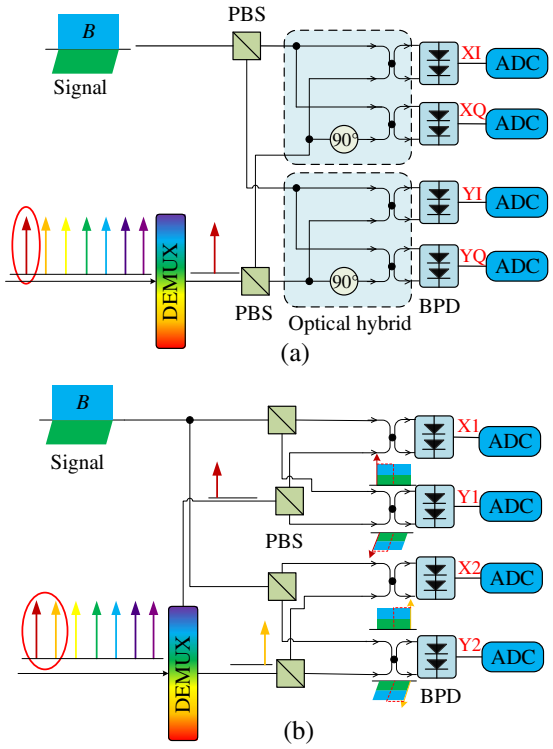

Fig. 1. Configuration of (a) the ICR and (b) the proposed SHCR in OFC-based architecture. ADC, analog-to-digital converter; DEMUX, demultiplexer; PBS, polarization beam splitter.

bandwidth, compared with traditional heterodyne detection, which requires a relatively high intermediate frequency (IF) that should be higher than the signal bandwidth. For instance, assuming that the bandwidth of a signal is B, the ICR only requires the electrical bandwidth of $B/2$ to recover the signal, while the traditional HCR requires the electrical bandwidth of B, which contributes to all the field-deployed coherent receivers being intradyne configurations.

The configuration of the proposed SHCR is shown in Fig. 1(b), where two comb lines with the same phase characteristics are demultiplexed through a wave-shaper or inter-leaver to serve as two LOs with different frequencies. After mixing two comb lines with optical signals in 2×2 couplers, respectively, the optical fields are square-law detected by four BPDs. The four channels from top to bottom in our proposed receiver are labeled as X1, Y1, X2, Y2, respectively. It is worth noting that we use four ADCs with only half of the signal bandwidth ($B/2$) to capture the waveforms, leading to a doubled electrical spectral efficiency in contrast to HCR. Only half of the spectrum information of the signal is received in each channel since the bandwidth of the ADC is $B/2$. Nevertheless, the signal spectrum in both polarizations has been completely captured thanks to the frequency spacing between two LOs. Compared with ICR, the 90° optical hybrids can be eliminated in the SHCR at the cost of two polarization beam splitters (PBSs) and five optical couplers.

In theory[14], based on 4×2 multiple-input-multiple-output (MIMO) equalization, the full spectrum in both X and Y polarizations could be recovered by combining the left-side part from X1, Y1 and the right side from X2, Y2. Thanks to the time-frequency property of the Fourier transform, the time-domain inter-symbol interference (ISI) is thus canceled. Therefore, we can recover all of the information of the signal through these four channels in the receiver DSP. The required electrical bandwidth of the ADC is reduced by half compared with HCR and the same as ICR. In the receiver DSP, after frequency offset estimation (FOE) and CD compensation, we combine the received signal from four channels at the equalization stage by 4×2 MIMO equalization, which is given by

$$x_{\text{out}}[k] = w_{x1-x}^{H}[k]x_1[k] + w_{x2-x}^{H}[k]x_2[k] + w_{y1-x}^{H}[k]y_1[k] + w_{y2-x}^{H}[k]y_2[k], \quad (1)$$

$$y_{\text{out}}[k] = w_{x1-y}^{H}[k]x_1[k] + w_{x2-y}^{H}[k]x_2[k] + w_{y1-y}^{H}[k]y_1[k] + w_{y2-y}^{H}[k]y_2[k], \quad (2)$$

where $x_1[k]$, $x_2[k]$, $y_1[k]$, and $y_2[k]$ denote the waveforms detected from channels X1, X2, Y1, and Y2, respectively. $w_{x1-x}[k]$, $w_{x2-x}[k]$, $w_{y1-x}[k]$, $w_{y2-x}[k]$, $w_{x1-y}[k]$, $w_{x2-y}[k]$, $w_{y1-y}[k]$, and $w_{y2-y}[k]$ are equalizers of MIMO, and $(\cdot)^H$ is the Hermitian operator.

To numerically verify the principle and feasibility of the proposed SHCR, we conduct simulations using commercial software VPItransmissionMaker. The 60 GBaud 16-QAM Nyquist

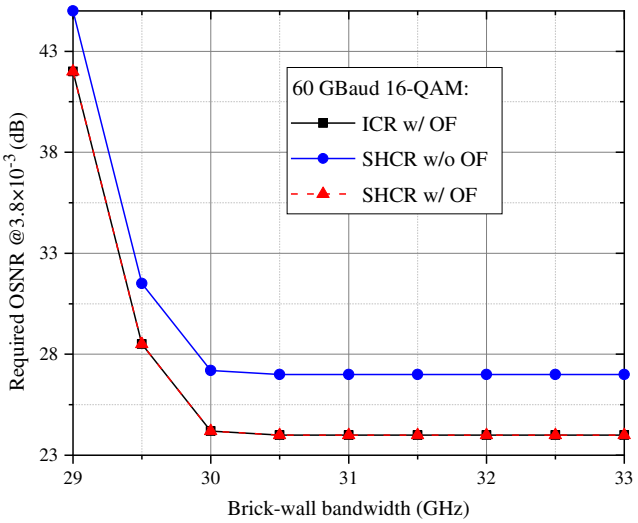

Fig. 2. Simulated OSNR sensitivity as a function of brick-wall electrical bandwidth in ICR and SHCR. OF, optical filter.

pulse with a 0.01 roll-off factor is generated, leading to 60.6 (=60 × 1.01) GHz bandwidth of the electrical signal.

We simulated the optical signal-to-noise ratio (OSNR) sensitivity as a function of the ADC bandwidth with a bit-error-rate (BER) below 7% hard-decision forward error correction (HD-FEC) of 3.8×10^{-3}, which is shown in Fig. 2. The LO power is defined as the power of a single comb line before photoelectric conversion. The LO power is set as 16 dBm to suppress SSBI, and PD noise is loaded into the signal including thermal noise, dark current, and shot noise. It can be observed that there is a 3 dB OSNR gap between ICR and HCR without an optical filter because the heterodyne detection suffers from the optical noise folding impact. Fortunately, the optical filter exists in the intra-DCI. Therefore, the 3 dB OSNR induced by optical noise folding can be removed. The OSNR sensitivity of both ICR and SHCR

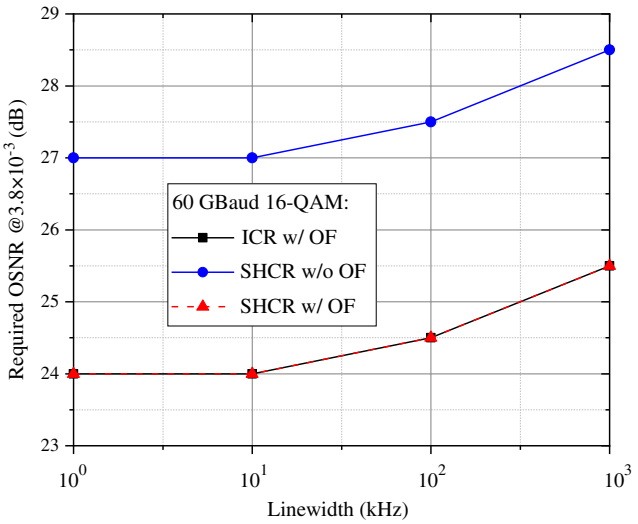

Fig. 3. Simulated OSNR sensitivity as a function of the different linewidths of the laser in ICR and SHCR. OF, optical filter.

degrade rapidly when electrical bandwidth is below the Nyquist bandwidth of 30.3 GHz in our cases. Therefore, the penalties resulting from electrical bandwidth are the same for both schemes.

Figure 3 depicts the OSNR sensitivity as a function of linewidth from 1 kHz to 1 MHz in the ICR and SHCR schemes. The linewidth increase from 100 kHz to 1 MHz does a large amount of damage to both receivers. The deterioration trend in OSNR sensitivity of the two receivers is the same, which indicates that SHCR also needs a narrow linewidth laser for coherent detection, and the phase noise imposes no extra penalty on the MIMO performance in SHCR.

3. Experimental Setup and DSP Procedures

We experimentally validate the principle of SHCR. As a proof-of-concept experiment, we demonstrate a single-polarization experiment here to illustrate the feasibility of the proposed SHCR scheme due to the lack of BPDs and a four-channel digital storage oscilloscope (DSO). The experimental setup of the proposed SHCR is depicted in Fig. 4. The DSP stacks of the transmitter and receiver are shown in Figs. 5(a) and 5(b), respectively. An external cavity laser (ECL) with ∼100 kHz linewidth is employed as the light source at the transmitter. An arbitrary waveform generator (Keysight M8194) with a 45 GHz electrical bandwidth operating at 120 GSa/s generates a 60 GBaud 16-QAM Nyquist pulse with a roll-off factor of 0.01. After being amplified by a dual-channel electrical amplifier (OA4SMM4), the IQ components of the complex-valued signal are loaded into an IQ modulator of 25 GHz 3 dB bandwidth biased at the null point to modulate the light from ECL1 (at 1542.14 nm). Then, the optical signal is amplified by an erbium-doped fiber amplifier (EDFA) and launched to an 80 km standard single-mode fiber (SSMF) with a launch power of 3 dBm.

At the receiver, the optical signal is amplified, filtered using an optical band-pass filter (OBPF), and then divided into two by a 1 × 2 coupler. The optical spectrum of the signal at stage (i) of Fig. 4 is shown in Fig. 6. The 31 GHz sinusoidal wave from the radio-frequency source (MXG N5183A) is fed into a Mach–Zehnder modulator (MZM) for two-tone LO generation at 1541.90 nm and 1542.39 nm. Then, the two comb lines are amplified by two EDFAs and filtered out by two OBPFs, respectively. Finally, the two LOs with a frequency gap of 62 GHz and 11 dBm power are obtained. We use polarization controllers to realize the polarization alignment of the signal and the two LOs, and then the two LOs are coupled together with two signal copies by two 2 × 2 optical couplers. The optical spectra at stage (ii) and stage (iii) of Fig. 4 are depicted in Fig. 6. Then, optical waveforms in these two channels are detected by two 43 GHz BPDs (FINISAR BPDV21x0R), and the photocurrents, labeled as X1 and X2, are captured by a real-time DSO with a 33 GHz brick-wall electrical bandwidth (Tektronix DPO75902SX) operating at 100 GSa/s for offline DSP.

The electrical spectra after resampling, FOE, and MIMO equalization are displayed in Figs. 7(a)–7(c), respectively. The

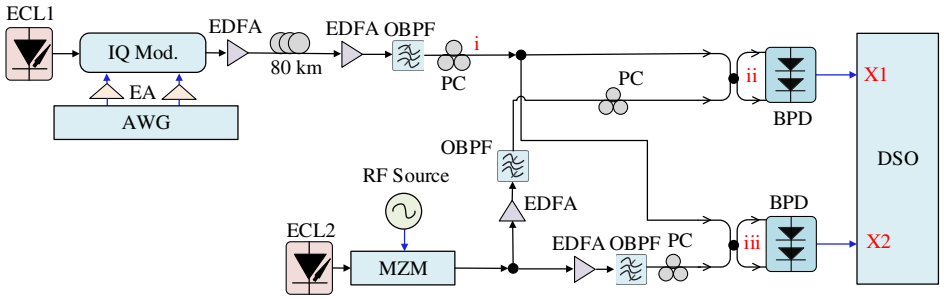

Fig. 4. Experimental setup of the SHCR. ECL, external cavity laser; AWG, arbitrary waveform generator; IQ Mod., IQ modulator; EA, electrical amplifier; EDFA, erbium-doped fiber amplifier; BPD, balanced photodetector; MZM, Mach–Zehnder modulator; OBPF, optical band-pass filter; PC, polarization controller; RF, radio frequency; DSO, digital storage oscilloscope.

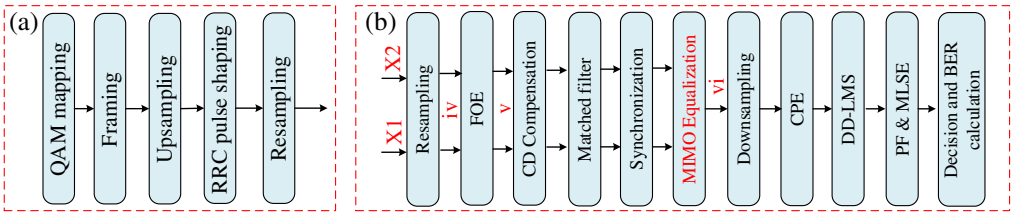

Fig. 5. (a) DSP stack at the transmitter. (b) DSP stack at the receiver. RRC, root raised cosine; FOE, frequency offset estimation; CPE, carrier phase recovery; DD-LMS, decision-directed least minimum square; PF, post filter; MLSE, maximum likelihood sequence estimation.

black electrical spectrum is from channel X1, corresponding to the black optical spectrum in Fig. 6, and the blue electrical spectrum corresponds to channel X2. At the receiver DSP, the two detected waveforms from X1 and X2 are firstly resampled to two sample-per-symbols (SPS). Then, the frequency offset between the transmitter laser and the two-tone LO is estimated based on the residual carrier generated by the drift of the IQ modulator bias point, which is circled in Fig. 7(a). FOE based on the residual carrier could further reduce the computational complexity of DSP. After CD compensation and matched filter, the two signals are fed into an MIMO equalizer operating at two SPS for ISI cancellation. As shown in Fig. 7(b), the electrical spectra after FOE only contain the left or right side of the signal spectrum information. However, thanks to the MIMO equalization, the complete spectrum is obtained by combining the left-side part from X1 and the right side from X2, as shown in Fig. 7(c). The taps of the MIMO equalizer are updated by the recursive least square (RLS) algorithm based on training sequences. After equalization, the carrier phase recovery based on the inserted pilot symbols and blind phase search[2] is conducted to eliminate phase noise. The percentage of the pilot symbols is 0.4%. Then, a decision-directed least minimum square (DD-LMS) equalizer is applied to correct residual ISI, and maximum likelihood sequence estimation (MLSE) with a post filter is used to whiten colored noise resulting from the equalizers.

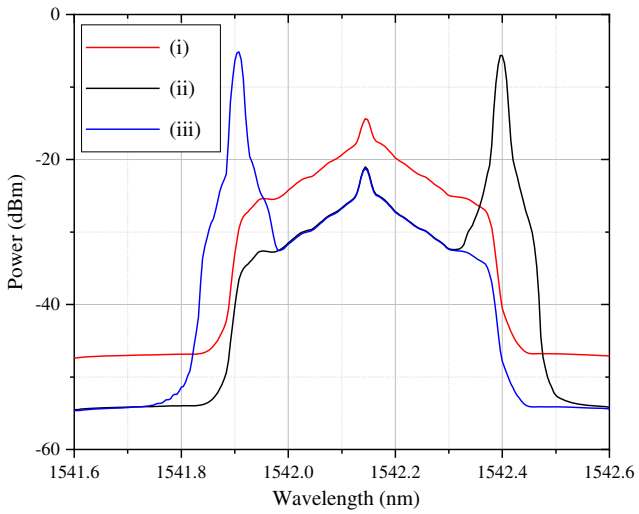

Fig. 6. Optical spectra of the signal at stages (i), (ii), and (iii) of Fig. 4.

4. Results and Discussion

The proposed SHCR has a skew between channels X1 and X2 from implementation, similar to the IQ skew in the ICR[2]. We first optimize the tap number of MIMO equalizers to obtain a moderate computational complexity and investigate the impact of skew induced by mismatched fiber length and cable on BER performance. We emulate skew between channels X1 and X2 in the receiver DSP. The results at the back-to-back (BTB) scenario are shown in Fig. 8. It can be observed that system performance remains stable until channel skew cannot be covered by the tap length of the equalizer. The skew tolerance could be calculated by

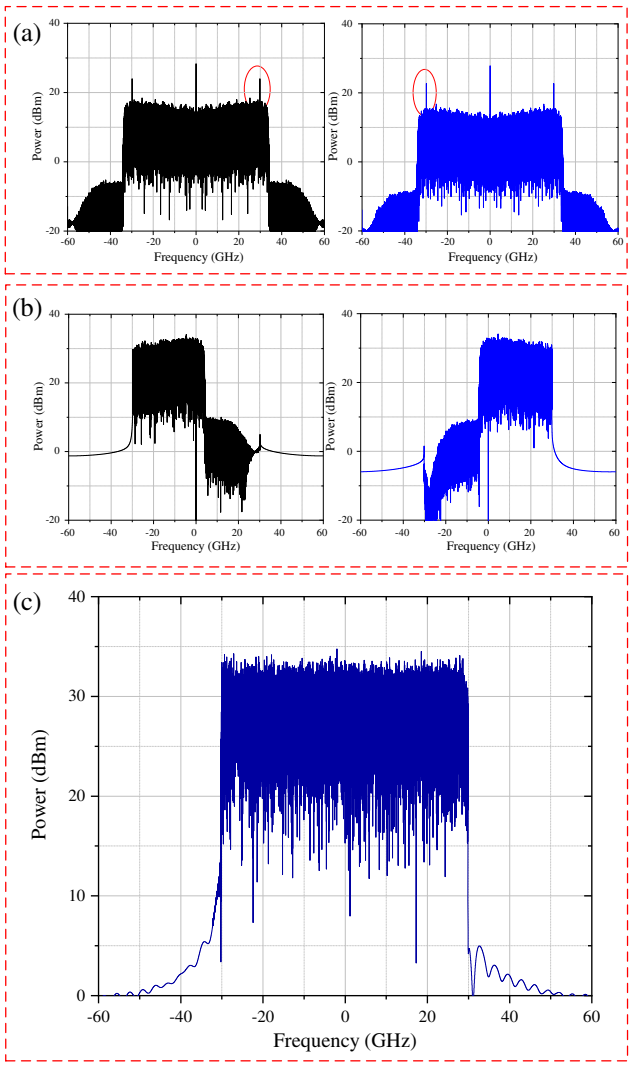

Fig. 7. Electrical spectra of the left- and right-side signal after (a) resampling, (b) FOE, and (c) MIMO equalization.

$$\text{skew tolerance} = (1/\text{sampling rate}) \times \text{tap number}. \quad (3)$$

The MIMO equalizer operates at two SPS, so the thresholds for the 20/30/40 taps equalizer are 166.67 ps, 250 ps, and 333.33 ps, respectively. Therefore, more filter taps indicate higher skew tolerance but also higher computational complexity. In the following context, we fix the number of taps as 30 to investigate bandwidth tolerance and the received optical power (ROP) of SHCR.

Then, we investigate the electrical bandwidth tolerance of SHCR. Figure 9 shows the BERs versus different brick-wall electrical bandwidths for a 60 GBaud 16-QAM at the BTB and 80 km SSMF transmission. As seen in Fig. 9, the BER performance deteriorates slowly with the electrical bandwidth decreasing from 33 GHz to 31 GHz since the frequency gap between two LOs is 62 GHz. The 31 GHz electrical bandwidth is sufficient for the ADCs and BPDs in the SHCR to obtain complete spectrum information to recover the original signal. As the electrical

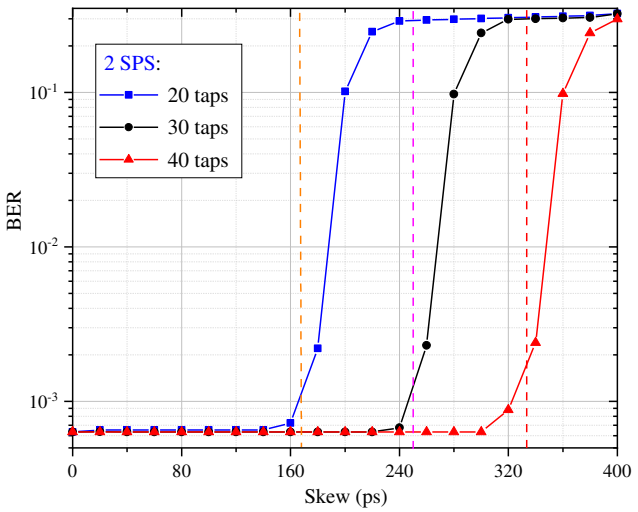

Fig. 8. Measured BER as a function of channel skew for 60-GBaud 16-QAM signal with the different number of equalizer taps.

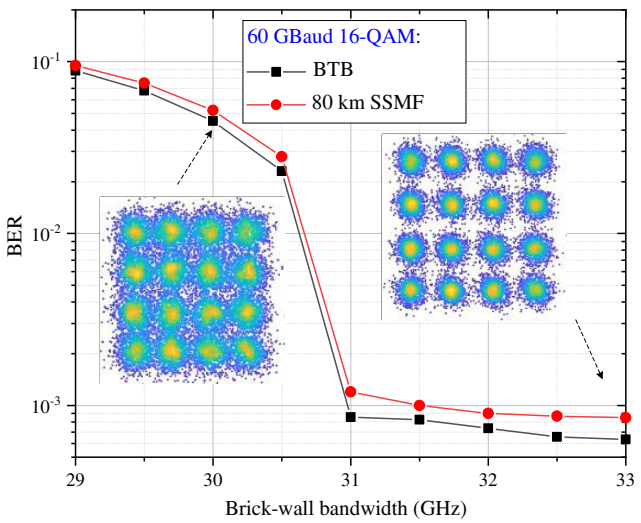

Fig. 9. Measured BER as a function of the brick-wall electrical bandwidth of the receiver for the 60 GBaud 16-QAM signal in the BTB case and 80 km SSMF transmission case.

bandwidth further decreases, part of the spectrum information is lost, which causes severe damage to signal recovery. The results in our experiments are highly consistent with the above simulation.

The measured BER versus ROP at BTB and 80 km SSMF transmission scenarios is displayed in Fig. 10. The optimal performance of the receiver is obtained at −4 dBm ROP. The corresponding BER is 6.2×10^{-4} below the 7% HD-FEC threshold of 3.8×10^{-3}. After 80 km SSMF transmission, there is a 1.2 dB sensitivity penalty at the BER threshold of 7% HD-FEC, part of which is caused by the amplified spontaneous emission noise of the EDFA. Note that the performance could be further improved by applying transimpedance amplifiers after the photodiodes.

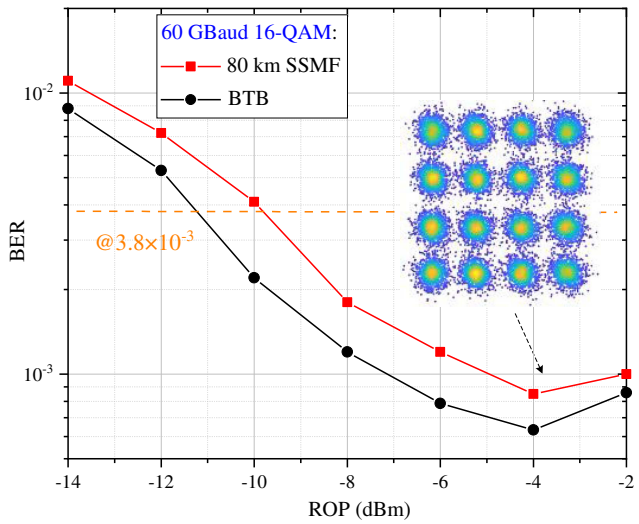

Fig. 10. Measured BER versus ROP for the 60 GBaud 16-QAM signal at the BTB and 80 km SSMF transmission cases.

The computational complexity of the DSP procedures used in the proposed SHCR is analyzed as follows. The residual carrier-assisted FOE only relies on Fourier transform and peak searching and exhibits lower complexity than the fourth power algorithm[2] used in ICR by saving the quadratic operation. As for static CD compensation and matched filtering, the DSP computational complexity of SHCR equals ICR since both SHCR and ICR conduct CD compensation and matched filtering on four real-valued channels, respectively. The complexity of SHCR and ICR in the equalization is the same because 4×2 MIMO equalization is also required in the ICR to obtain a good tolerance against IQ skew. Moreover, the DSP of SHCR after the MIMO equalization is also used in the ICR. In summary, SHCR does not bring additional computational complexity on the DSP aspect with respect to ICR.

5. Conclusion

In this work, we propose a spectrally sliced coherent detection scheme called SHCR to improve the tolerance to electrical bandwidth in the heterodyne coherent detection. The key idea of the proposed SHCR is to employ spectrally sliced detection and MIMO equalization to complete full spectrum recovery. The performance of the SHCR scheme is numerically compared with ICR. A 60 GBaud Nyquist 16-QAM transmission over 80 km SSMF is experimentally demonstrated to validate its principle and feasibility. The SHCR shows good tolerance to laser linewidth, fiber dispersion, channel skew, and electrical bandwidth based on the numerical and experimental results. This is the first, to the best of our knowledge, realization of heterodyne detection with a low receiver bandwidth at almost half of the baud rate.

Acknowledgement

This work was supported by the National Natural Science Foundation of China (No. 62001287) and National Key R&D Program of China (No. 2018YFB1800904).

References

1. S. Tsukamoto, D. Ly-Gagnon, K. Katoh, and K. Kikuchi, "Coherent demodulation of 40-Gbit/s polarization-multiplexed QPSK signals with 16-GHz spacing after 200-km transmission," in *Optical Fiber Communication Conference* (2005), paper PDP29.
2. K. Kikuchi, "Fundamentals of coherent optical fiber communications," J. Light. Technol. **34**, 157 (2016).
3. K. Kikuchi and S. Tsukamoto, "Evaluation of sensitivity of the digital coherent receiver," J. Light. Technol. **26**, 1817 (2008).
4. S. Lu, Y. Zhou, F. Zhu, J. Sun, Y. Yang, R. Zhu, S. Hu, X. Zhang, X. Zhu, X. Hou, and W. Chen, "Digital-analog hybrid optical phase-lock loop for optical quadrature phase-shift keying," Chin. Opt. Lett. **18**, 090602 (2020).
5. S. J. Savory, "Digital filters for coherent optical receivers," Opt. Express **16**, 804 (2008).
6. X. Zhou, J. Yu, and D. Qian, "A novel DSP algorithm for improving the performance of digital coherent receiver using single-ended photo detection," in *European Conference on Optical Communication* (2008), paper Mo4D.1.
7. S. T. Le, V. Aref, J. Cho, X. Chen, and D. Che, "882 Gbps transmission over 100 km of SSMF using a self-calibrated single-ended coherent receiver," in *Optical Fiber Communication Conference* (2021), paper M3I.2.
8. C. Xie, P. J. Winzer, G. Raybon, A. H. Gnauck, B. Y. Zhu, T. Geisler, and B. Edvold, "Colorless coherent receiver using 3×3 coupler hybrids and single-ended detection," Opt. Express **20**, 1164 (2012).
9. J. Zhang, Z. Dong, J. Yu, N. Chi, L. Tao, X. Li, and Y. Shao, "Simplified coherent receiver with heterodyne detection of eight-channel 50 Gb/s PDM-QPSK WDM signal after 1040 km SMF-28 transmission," Opt. Lett. **37**, 4050 (2012).
10. X. Li, J. Yu, N. Chi, Z. Dong, J. Zhang, and J. Yu, "The reduction of the LO number for heterodyne coherent detection," Opt. Express **20**, 29613 (2012).
11. W. Shieh, C. Sun, and H. Ji, "Carrier-assisted differential detection," Light Sci. Appl. **9**, 18 (2020).
12. S. Kumar, G. Papen, K. Schmidtke, and C. Xie, "Intra-data center interconnects, networking, and architectures," in *Optical Fiber Telecommunications VII* (Elsevier, 2020), p. 627.
13. H. Hu and L. K. Oxenløwe, "Chip-based optical frequency combs for high-capacity optical communications," Nanophotonics **10**, 1367 (2021).
14. N. K. Fontaine, R. P. Scott, L. Zhou, F. M. Soares, J. P. Heritage, and S. J. B. Yoo, "Real-time full-field arbitrary optical waveform measurement," Nat. Photonics **4**, 248 (2010).